Optics and Laser Technology 106 (2018) 372–377

Contents lists available at ScienceDirect

Optics and Laser Technology

journal homepage: www.elsevier.com/locate/optlastec

Full length article

Investigation on picosecond laser-induced damage in HfO_2/SiO_2 high-reflective coatings

Cheng Li [a,b], Yuan'an Zhao [a,d,*], Yun Cui [a], Yueliang Wang [a,b], Xiaocong Peng [a,b], Chong Shan [a,c], Meiping Zhu [a], Jianguo Wang [a], Jianda Shao [a]

[a] Laboratory of Thin Film Optics, Key Laboratory of Materials for High Power Laser, Shanghai Institute of Optics and Fine Mechanics, Chinese Academy of Sciences, Shanghai 201800, China
[b] University of Chinese Academy of Sciences, Beijing 100049, China
[c] Changchun University of Science and Technology, Changchun 130022, China
[d] Changchun Institute of Optics, Fine Mechanics and Physics, Chinese Academy of Sciences, China

ARTICLE INFO

Article history:
Received 6 January 2018
Received in revised form 18 April 2018
Accepted 25 April 2018

Keywords:
High-reflective coating
Laser-induced damage
Protective layer
Picosecond pulse
Electric field distribution

ABSTRACT

We investigate the influence of a protective layer on the picosecond laser-induced damage in HfO_2/SiO_2 high-reflective (HR) coatings. Two types of 1064-nm HR coatings, with and without a SiO_2 protective layer, are deposited using electron beam evaporation. Laser-induced damage tests are operated with 1064-nm, 30-ps laser pulses in one-on-one mode. Five different angles of incidence (AOIs) are considered in the tests for both coatings, in order to modulate the electric field (*E*-field) intensity in the HR coatings. The damage morphologies and cross-sections of the damage sites are characterized using scanning electron microscope (SEM) and focused ion beam (FIB), respectively. Experimental results show that the SiO_2 protective layer slightly improves the laser-induced damage threshold (LIDT) of the HR coatings for all AOI values. The damage morphology contains high-density micrometer-scale pits and layer delaminations, at low and high fluences, respectively. The cross-sections of the damage sites and LIDTs for different AOIs are compared with corresponding *E*-field distributions. For both coatings, the damage is initiated near the peak of the *E*-field. A negative linear relationship is observed between the LIDT and corresponding maximum *E*-field intensity for both coatings.

1. Introduction

Laser-induced damage in optical components has always been a key challenge in the development of high-power laser systems. Extensive experimental and theoretical studies have been performed to reveal the damage mechanisms of optical components. The results showed that the damage mechanisms depend on the pulse duration. In the nanosecond regime, the localized absorption of incident radiation by isolated defects or impurities in the material, is transferred to the lattice. Damage occurs when the heat deposited near absorption centers is sufficiently high to melt, boil, or fracture the host material [1,2]. A τ^x-dependence of the threshold damage fluence, where τ is the pulse duration, has been observed in numerous experiments, with x in the range of 0.3–0.6 for different dielectric materials, for pulses longer than 20 ps [3–5]. In the femtosecond regime, laser-induced damage can be explained by multiphoton absorption and impact ionization, which depend on the local intensity enhancements in the material, determined by intrinsic material properties rather than impurities or defects [1,6,7]. However, the mechanism of laser damage in the picosecond regime is not yet understood, and the laser–matter interactions are quite complex in this regime.

Along with the studies on damage mechanisms, researchers design optical components according to their discrepant damage resistance in different laser applications. Typically, for multilayer HR coatings, different coating stacks are designed for different pulse durations. In the nanosecond regime, the main reason of laser-induced damage is attributed to the heat generated from the laser beam absorption by inclusions, accumulated in the surrounding host material [8]. A half-wave single protective layer consist of low refractive index dielectric material on the top of coating stacks can efficiently improve the laser-induced damage threshold (LIDT) [9,10]. The protective layer can adjust the temperature distribution in the coating stacks and lower the thermal response [11]. However, in the femtosecond regime, the protective layer decreases the LIDT of HR coatings with the increase of electric field

* Corresponding author at: Laboratory of Thin Film Optics, Key Laboratory of Materials for High Power Laser, Shanghai Institute of Optics and Fine Mechanics, Chinese Academy of Sciences, Shanghai 201800, China.
E-mail address: yazhao@siom.ac.cn (Y. Zhao).

https://doi.org/10.1016/j.optlastec.2018.04.028
0030-3992/

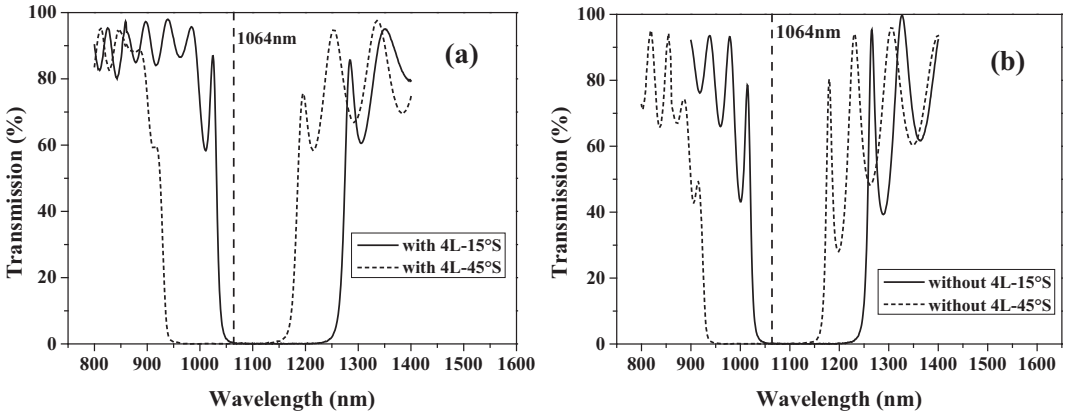

Fig. 1. Spectra of the coatings (a) without and (b) with a 4L protective layers, for AOIs of 15° and 45°.

(*E*-field) intensity in the coatings [12]. Therefore, we focus on the influence of protective layer on the picosecond laser-induced damage behaviors in HfO_2/SiO_2 HR coatings.

In this study, the damage thresholds of two HR coatings, with and without a SiO_2 protective layer, are tested using picosecond pulses with different testing conditions. The testing results are compared and the origin of the damage is discussed.

2. Experimental methods

Two types of HR coating, with and without a SiO_2 protective layer, were prepared. The coating stacks of two HR coatings were G|4L(HL)^{15}H4L and G|4L(HL)^{15}H, where G represents the K9 substrate, while L and H denote low (SiO_2) and high (HfO_2) refractive-index materials, with a quarter-wavelength optical thickness (QWOT), respectively. Both coatings were designed for the wavelength of 1064 nm with AOI of 45°, deposited using electron beam evaporation. For the LIDT tests, a 1064-nm Nd:YAG laser (PL2143B, Ekspla) was employed. The linearly polarized output laser beam has a maximum energy of 5 mJ, pulse width of 30 ps, and repetition rate of 10 Hz. The LIDT tests were performed in one-on-one mode; S-polarized pulses with five different AOIs of 15°, 22°, 30°, 37°, and 45° were employed in the tests to modulate the *E*-field intensity in the HR coatings. For all AOIs, the employed laser wavelength of 1064 nm was in the reflection band. Fig. 1 shows the spectral curves for AOIs of 15° and 45°.

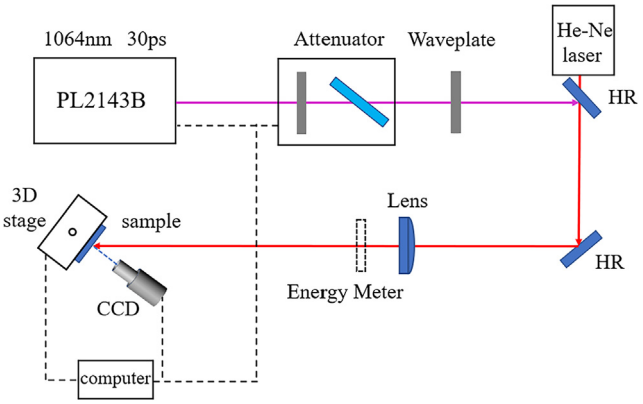

Fig. 2. Schematic illustration of the experimental setup.

The experimental setup is illustrated in Fig. 2. A λ/2-plate combined with a polarizing beam splitter acted as an attenuator to modulate the laser energy. Another λ/2-plate placed downstream from the attenuator was employed to change the polarization. The samples were mounted on a motorized *x*-*z* rotation stage and positioned at the focal plane of the lens with a focal length of 750 mm. The pulse energy was measured in the main path with an energy meter for each energy step prior to the tests; the $\omega_{1/e}^2$ spot size at the focus was 230 ± 10 μm, measured by a laser beam profiler. In-situ imaging of the front surface of the samples combined with ex-situ optical microscope observation were employed to monitor the occurrence of damage; a He-Ne laser beam overlapped with the main path was employed to assist the monitoring. Any change in the samples caused by the laser irradiation was regarded as damage.

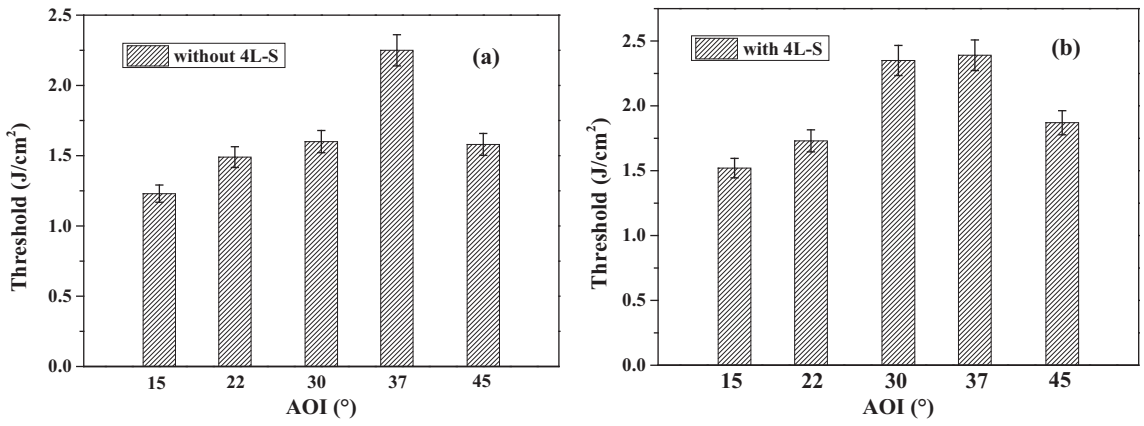

Fig. 3. Damage thresholds of the coatings (a) without and (b) with a 4L protective layers, for five different AOIs.

3. Results and discussion

Fig. 3 shows the LIDTs of the two types of coatings, obtained for five different AOIs. For all five AOIs, the protective layer increases the LIDT to a certain extent; the LIDTs of both coatings vary with the AOI with a similar trend. Damage morphologies of both coatings are shown in Fig. 4. The damage sites can be classified into two typical morphologies, caused by significantly different laser fluences. At a low fluence, the damage morphology contains high-density pits with sizes of several micrometers; slight differences in the pits can be observed between the two coatings. For the coating without the protective layer, the damage sites consist of a mass of ripple-like pits accompanied by some much smaller, tiny pits. For the coating with the protective layer, the pits have a larger size and show ripple-like or flat-pit morphologies. The pits morphologies do not vary with the AOI, as illustrated in Fig. 4. At a high laser fluence, all of the damage sites suffered a layer delamination; the newly exposed inner layers have no pits. In addition, high-density pits, which resemble those of the low-fluence morphology, emerge around the boundaries of the damage area; it is

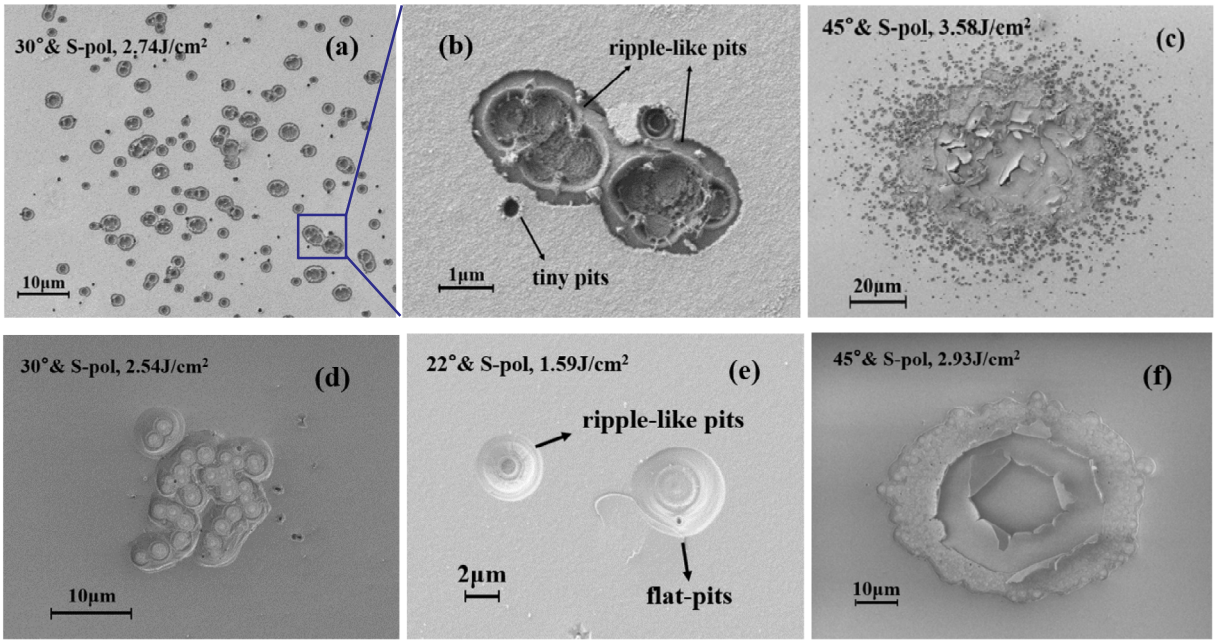

Fig. 4. Typical damage morphologies of the coatings (a–c) without and (d–f) with a 4L protective layer. (b) Magnified view of a feature in (a). In (b) and (e), ripple-like and tiny or flat pits are marked, respectively.

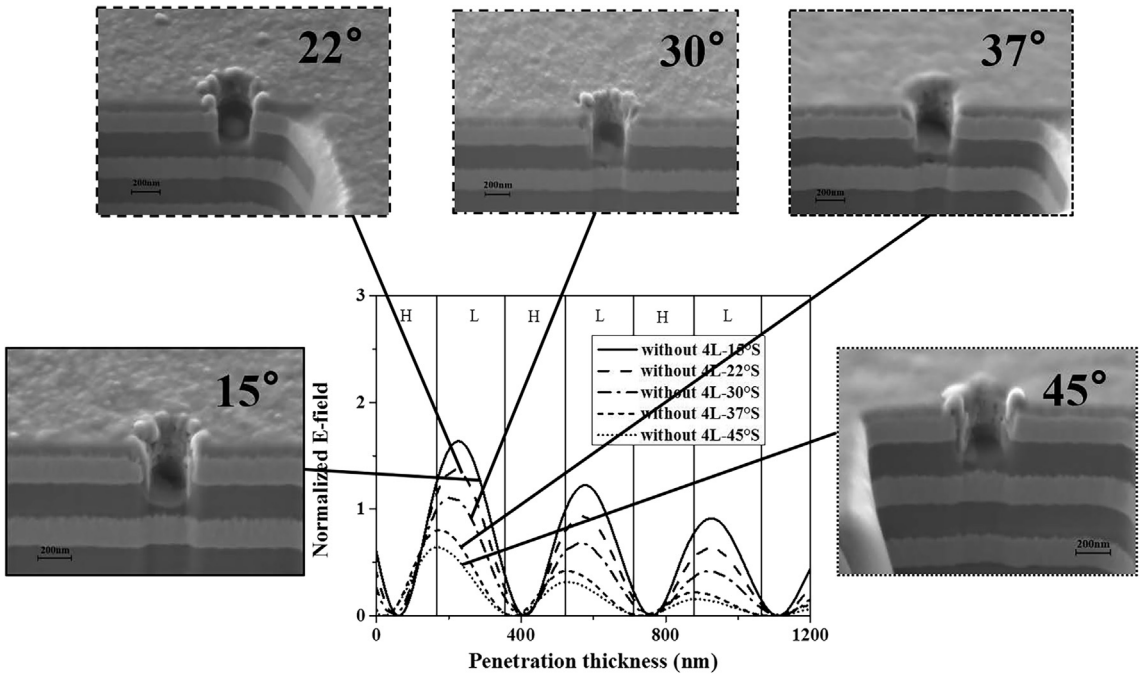

Fig. 5. Cross-sections of tiny pits of the coatings without a 4L protective layer, for different AOIs. Damage locations are marked in the corresponding positions of the *E*-field.

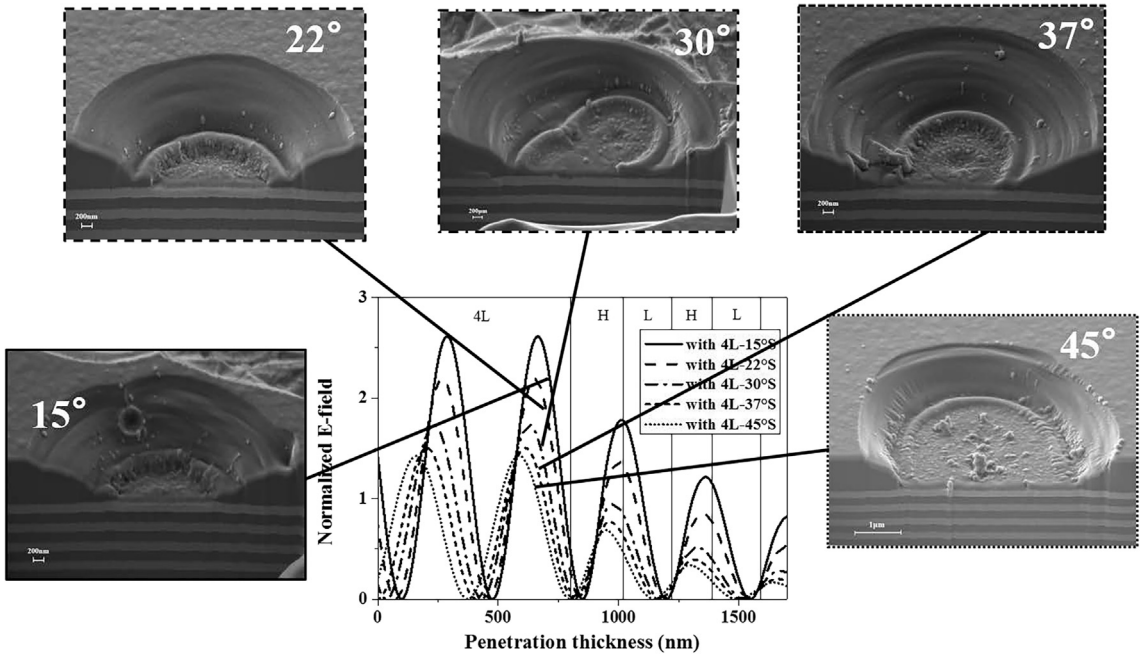

Fig. 6. Cross-sections of flat pits of the coatings with a 4L protective layer, for different AOIs. Damage locations are marked in the corresponding positions of the *E*-field.

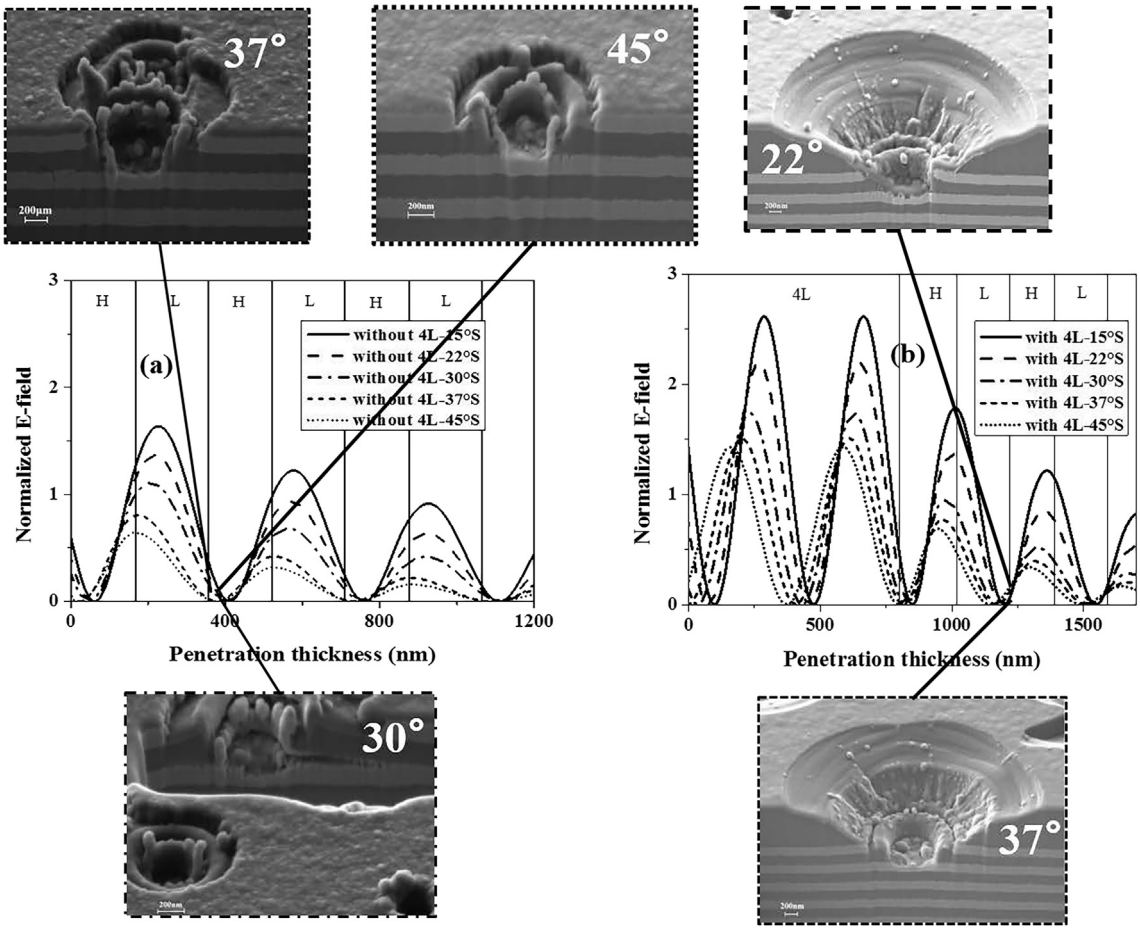

Fig. 7. Cross-sections of ripple-like pits of the coatings (a) without and (b) with a 4L protective layers, for different AOIs. Damage locations are marked in the corresponding positions of the *E*-field.

likely that they emerge owing to the low fluence around the boundaries of the Gaussian beam.

More detailed cross-section images, obtained by focused ion beam, are shown in Figs. 5–7. We investigated the onset of laser damage, and compared the cross-section images with the corresponding *E*-field distributions for different AOIs, calculated by a thin-film design software, as illustrated in Figs. 5–7. Figs. 5 and 6 show the damage locations of the tiny and flat pits, respectively, while Fig. 7 shows the damage locations of the ripple-like pits. The results suggest that for both coatings, the ripple-like pits locate at the first L/H interface for all AOIs, close to the position of the minimum of the *E*-field. In contrast, the tiny pits locate at the first SiO_2 layer, while the flat pits locate at the 4L protective layer, both near the position of the peak of the *E*-field. Therefore, the tiny and flat pits are likely to correspond to the damage onsets of the two coatings, owing to the *E*-field dependence in the damage locations. The ripple-like pits represent the following stage of the damage development, independent of the *E*-field, located deeper than the onset damage sites. In order to verify these claims, we investigated the relationship between the LIDTs for different AOIs and corresponding maximum *E*-intensities in the coating stacks; the results are shown in Fig. 8. A negative linear relationship can be observed between the LIDT and corresponding maximum *E*-intensity, for both coatings. Based on the above results, we can conclude that the damages in both coatings are *E*-field-induced damages.

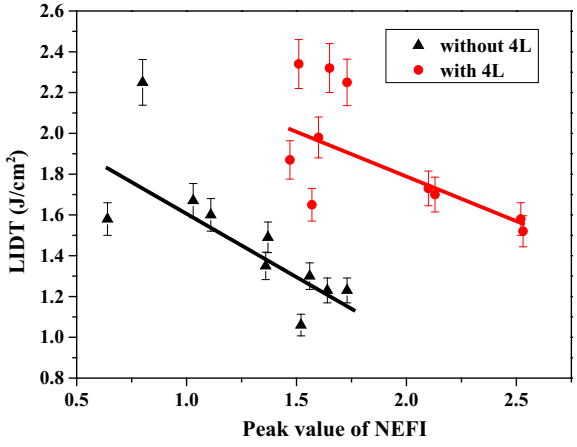

Fig. 8. LIDT as a function of corresponding maximum *E*-field. circular and triangle dots represent the results for the coatings with and without a protective layer, respectively; the lines represent the fitting curves.

The high-density pits suggest that the damage progress can be linked to the localized absorbers, typically defects and impurities; they induce damage in the nanosecond regime. We aim to reveal the damage mechanisms for the two coatings. First, we measured the thermal absorption. Thermal lensing technique with a 1064-nm continuous-wave (CW) laser was employed; the incident angle of the pump laser beam was varied. Thermal lensing is generated when a material is irradiated by a laser beam, the heat generated from the laser irradiation diffuses in the material, and causes a radial thermal gradient. The temperature variations within the material cause thermal distortions of the laser beam, owing to the temperature- and stress-dependent variations of the refractive index [13]. The thermal lensing limits the output power of the high-power laser [14]; however, it is effective for the measurement and analysis of weak-absorption optical coatings [15]. The principles of the thermal lensing technique and its specific experimental setup are described by Xu et al. [15]. Fig. 9 shows that the thermal absorptions of the two coatings are very low, one-on-one test and raster scan were then performed using 1064-nm 9.8-ns pulses. Raster scan is another damage test method, different from the one-on-one mode. In the process of raster scan, a stationary laser beam with a certain repetition frequency scans the surface of the tested sample, mounted on a motion stage. The movement speed of the sample can be adjusted so that the step size between adjacent pulses is equal to the laser beam diameter at 90% of the peak fluence; therefore, the entire surface is exposed with 90% of the peak laser fluence. An online video system was employed to observe the surface of the tested sample; the damage density could be obtained after the test. The setup of the raster scan is described in Refs. [16,17]. In our experiment, four 1 cm × 1 cm areas were scanned using four different fluences of 25, 40, 60, and 80 J/cm^2; the corresponding damage densities were 9, 5, 17, and 15 cm^{-2}, respectively, significantly lower than the density of pits obtained with picosecond pulses. The morphologies obtained during the raster scan (Fig. 10) are typical plasma scalds and nodular-ejection pits, different from the morphology obtained using 30-ps pulses. The damage probability of the one-on-one test is shown in Fig. 11. The coating exhibited a very low damage probability, even for fluences up to 80 J/cm^2, which matched the low damage density obtained with the raster scan. Therefore, thermal absorption defects should not be regarded as damage initiators in the picosecond regime. The damage mechanisms which provide such type of high-density pits are still under investigated. Similar damage morphologies in HR coatings obtained using 351-nm, 0.7-ns pulses were reported by Papernov [18], few-nanometer-sized metal clusters and high-density areas of electronic defects were identified as the damage initiators [19].

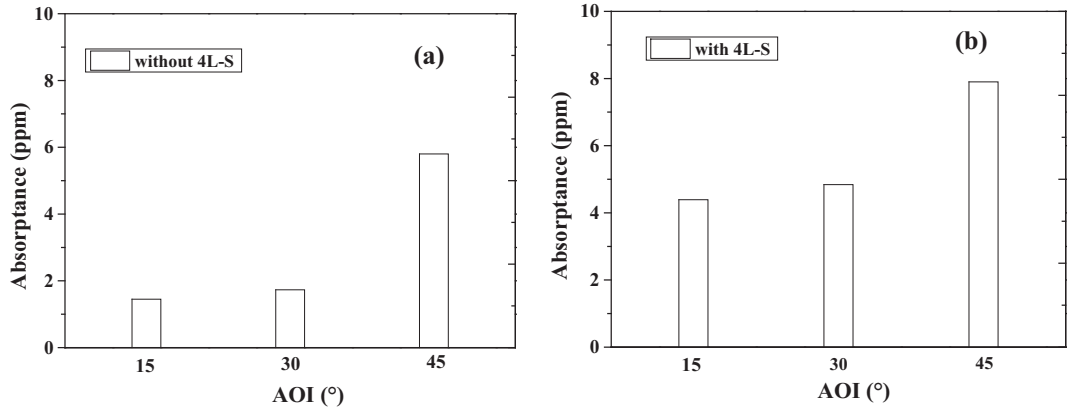

Fig. 9. Thermal absorptions of the coatings (a) without and (b) with a protective layer, for different AOIs.

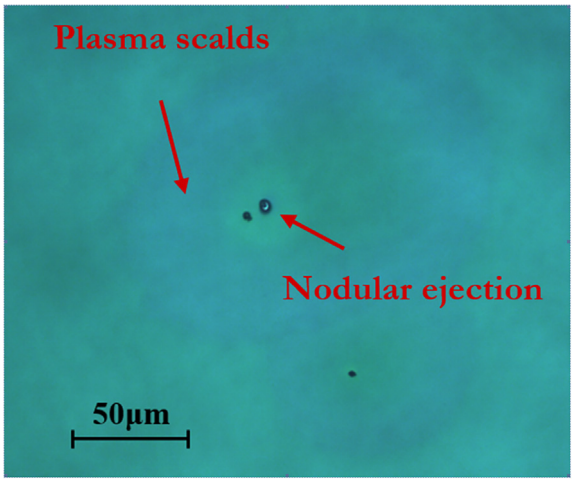

Fig. 10. Morphology of a damage site obtained by raster scan.

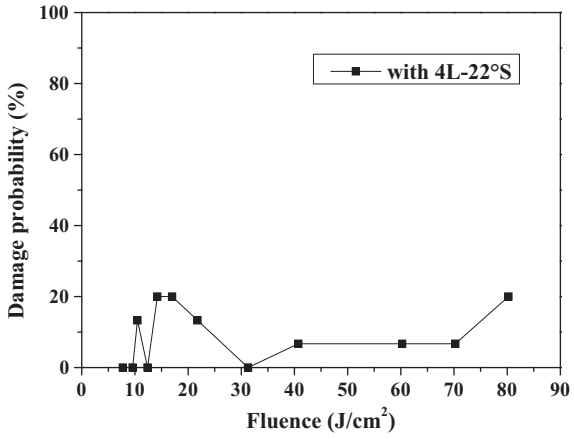

Fig. 11. One-on-one damage probability of the coating vs. laser fluence, obtained with nanosecond pulses.

4. Conclusion

The damages of two different types of HfO_2/SiO_2 HR coatings with and without a SiO_2 protective layer, obtained by picosecond laser pulses, were investigated. The results showed that the protective layer can increase the LIDT of the HR coating to a certain extent. The damage morphologies of the two coatings are slightly different; however, for each coating, the damage onsets for different AOIs are in the same layer, near the peak of the *E*-field. A negative linear relationship was observed between the LIDT and corresponding maximum *E*-field intensity, for both coatings. Therefore, the damages which occurred in the two coatings are likely to be *E*-field-dependent. The damage morphologies of the two coatings indicated that the damages were initiated at high-density isolated absorbers, which may be few-nanometer-sized metal clusters or high-density areas of electronic defects, as observed in similar morphologies reported by Papernov et al. [18,19].

Acknowledgements

This study was supported by the Chinese National Natural Science Foundation and NSAF (Grant No. U1430121).

References

[1] B.C. Stuart, M.D. Feit, S. Herman, A.M. Rubenchik, B.W. Shore, M.D. Perry, Nanosecond-to-femtosecond laser-induced breakdown in dielectrics, Phys. Rev. B 53 (4) (1996) 1749–1761.
[2] Y. Zheng, L. Ding, X. Zhou, R. Ba, J. Yuan, H. Xu, X. Yang, B. Chen, J. Na, Y. Li, W. Zheng, Preliminary study of the damage resistance of type I doubler KDP crystals at 532 nm, Chin. Opt. Lett 14 (5) (2016) 051601.
[3] D. Du, X. Liu, G. Korn, J. Squier, G. Mourou, Laser-induced breakdown by impact ionization in SiO_2 with pulse widths from 7 ns to 150 fs, Appl. Phys. Lett 64 (23) (1994) 3071–3073.
[4] C.W. Carr, J.B. Trenholme, M.L. Spaeth, Effect of temporal pulse shape on optical damage, Appl. Phys. Lett 90 (4) (2007) 041110.
[5] D.A. Alessi, C.W. Carr, R.P. Hackel, R.A. Negres, K. Stanion, J.E. Fair, D.A. Cross, J. Nissen, R. Luthi, G. Guss, J.A. Britten, W.H. Gourdin, C. Haefner, Picosecond laser damage performance assessment of multilayer dielectric gratings in vacuum, Opt. Express 23 (12) (2015) 15532–15544.
[6] J. Jasapara, A.V.V. Nampoothiri, W. Rudolph, D. Ristau, K. Starke, Femtosecond laser pulse induced breakdown in dielectric thin films, Phys. Rev. B 63 (4) (2001) 045117.
[7] A.C. Tien, S. Backus, H. Kapteyn, M. Murnane, G. Mourou, Short-pulse laser damage in transparent materials as a function of pulse duration, Phys. Rev. Lett. 82 (19) (1999) 3883–3886.
[8] A.A. Manenkov, Fundamental mechanisms of laser-induced damage in optical materials: today's state of understanding and problems, Opt. Eng 53 (1) (2014) 010901.
[9] F. Rainer, W.H. Lowdermilk, D. Milam, T.T. Hart, T.L. Lichtenstein, C.K. Carniglia, Scandium oxide coatings for high-power UV laser applications, Appl. Opt 21 (20) (1982) 3685–3688.
[10] M. Zhan, H. He, Y. Zhao, G. Tian, J. Shao, Z. Fan, Overcoat dependence of laser-induced damage threshold of 355nm HR coatings, Appl. Surf. Sci 252 (6) (2006) 2126–2130.
[11] C.J. Stolz, F.Y. Genin, T.A. Reitter, N.E. Molau, R.P. Bevis, M.K.V. Gunten, D.J. Smith, J.F. Anzellotti, Effect of SiO_2 overcoat thickness on laser damage morphology of HfO_2, SiO_2 Brewster's angle polarizers at, 1064nm, Proc. SPIE 2966 (1997) 265–272.
[12] L. Yuan, Y. Zhao, C. Wang, H. He, Z. Fan, J. Shao, Effect of SiO_2 protective layer on the femtosecond laser-induced damage of HfO_2/SiO_2 multilayer high-reflective coatings, Appl. Surf. Sci. 253 (7) (2007) 3450–3454.
[13] W. Koechner, Thermal lensing in a Nd: YAG laser rod, Appl. Opt 9 (11) (1970) 2548–2553.
[14] S.H. Noh, D.J. Kim, J.W. Kim, High power generation of adaptive laser beams in a Nd: YVO_4 MOPA system, Chin. Opt. Lett 15 (12) (2017) 120801.
[15] J. Xu, M. Zhu, Y. Zhao, K. Yi, J. Shao, Photothermal tomography of optical coatings based on surface thermal lensing technology, Proc. of SPIE 8190 (2011) 819010.
[16] Y. Zhao, T. Wang, D. Zhang, S. Fan, J. Shao, Z. Fan, Laser conditioning of ZrO_2: Y_2O_3/SiO_2 mirror coatings prepared by E-beam evaporation, Appl. Phys. Lett 239 (2) (2005) 171–175.
[17] L.M. Sheehan, M.R. Kozlowski, F. Rainer, M.C. Staggs, Large-area conditioning of optics for high-power laser systems, 2114 (1994) 559-569.
[18] S. Papernov, A.W. Schmid, Localized absorption effects during 351 nm, pulsed laser irradiation of dielectric multilayer thin films, J. Appl. Phys. 82 (11) (1997) 5422–5432.
[19] S. Papernov, A. Tait, W. Bittle, A.W. Schmid, J.B. Oliver, P. Kupinski, Near-ultraviolet absorption and nanosecond-pulse-laser damage in HfO_2 monolayers studied by submicrometer-resolution photothermal heterodyne imaging and atomic force microscopy, J. Appl. Phys. 09 (11) (2011) 113106.